# COS-B VIEWS ON THE DIFFUSE GALACTIC GAMMA-RAY EMISSION AND SOME POINT SOURCES

W. HERMSEN

*Laboratory for Space Research Leiden, P.O. Box 9504, 2300 RA Leiden, The Netherlands*

(Received 1 June, 1988)

**Abstract.** The correlation between diffuse galactic gamma rays and gas tracers is studied using the final COS-B database and H I and CO surveys covering the entire galactic plane. A good quantitative fit to the gamma rays is obtained, with a small galacto-centric gradient in the gamma-ray emissivity per hydrogen atom. The average ratio of $H_2$ column density to integrated CO temperature is determined, the best estimate being $(2.3 \pm 0.3) \times 10^2$ molecules $cm^{-2}$ $(K\ km\ s^{-1})^{-1}$. Strictly taken, this value is an upper limit. The corresponding mass of molecular hydrogen in the inner galaxy, derived using both 1st and 4th quadrants, is $1.0 \times 10^9\ M_\odot$.

The softer gamma-ray spectrum towards the inner galaxy found in previous work can be attributed to a steeper emissivity gradient at low energies and/or to a softer gamma-ray spectrum of the emission distributed like molecular gas. A steeper emissivity gradient at low energies could be related to cosmic-ray spectral variations in the Galaxy, to different distributions of cosmic-ray electrons and nuclei, or to a contribution from discrete sources. A softer spectrum for the emission associated with molecular clouds may be physically related to the clouds themselves (i.e., cosmic-ray spectral variations) or to an associated discrete source distribution.

New results on the temporal and spectral characteristics of the high-energy (50 MeV to 5 GeV) gamma-ray emission from the Vela pulsar are presented. The whole pulsed flux is found to exhibit long-term variability. Five discrete emission regions within the pulsar lightcurve have been identified, with the spectral characteristics and long-term behaviour being different. These characteristics differ significantly from those reported earlier for the Crab pulsar. However, geometrical pulsar models have been proposed (e.g., Morini, 1983; Smith, 1986) which could explain many of these features.

## 1. Introduction

The good quantitative correlation between galactic gamma-rays and gas tracers (H I and CO emission) in the Galaxy is the main evidence that interactions of cosmic rays with interstellar gas are responsible for most of the galactic gamma-ray emission for energies between 100 MeV and a few GeV. Prior to 1982 it was impossible fully to exploit this correlation for lack of adequate coverage in the CO surveys, required to estimate the galactic distribution of molecular hydrogen. The situation improved dramatically with the availability of the large-scale 'superbeam' survey in CO from the Columbia 1.2 m telescopes, first only from New York City, later also on Cerro Tololo in Chile. These surveys, combined for the large-scale panorama presented by Dame *et al.* (1987), provide complete sampling over a large enough latitude range to allow a reliable comparison with the gamma-ray data.

In the third paper of a series of four, Bloemen *et al.* (1986) used low-latitude COS-B data taken from the first 55 (out of 65) observation periods together with the 1st and 2nd quadrant and Carina Colombia CO surveys, and various H I surveys. The gas surveys were first divided into galacto-centric distance bins using the rotation curves of

*Space Science Reviews* **49** (1988) 17–39.

Gordon and Burton (1976) and Blitz *et al.* (1980), as modified by Kulkarni *et al.* (1982): the bins chosen were 2–8, 8–10, 10–15, and $> 15$ kpc. The main result was the determination of the gamma-ray emissivity gradient in the three energy ranges, the establishment of the requirement for an energy-dependent model, and the derivation of a value for the CO-to-$H_2$ conversion factor together with a new estimate for the mass of molecular hydrogen in the inner galaxy. The emissivity gradients were found to be surprisingly small, especially at high energies ($> 300$ MeV), when compared to the distribution of candidate cosmic-ray sources in the Galaxy (see, e.g., Dogiel and Uryson, 1988). In this paper, Section 2, the results of the fourth paper of the series (Strong *et al.*, 1988) are summarized. The improvements over the analysis of Bloemen *et al.* (1986) include the availability of the total COS-B database with its final calibration and the updating of the CO database. The latter covers now the entire longitude range and allows the analysis of a greater latitude range ($|b| < 9.5°$) than before.

Despite the good quantitative correlation between the galactic gamma rays and the gas tracers, there are evident discrepancies due to the presence of gamma-ray point sources, such as the well-known Crab and Vela pulsars, Geminga (2CG195 + 04), and the strong unidentified source in the Cygnus region (2CG078 + 01). These sources are all contained in the 2CG catalogue (Swanenburg *et al.*, 1981), which was compiled prior to the availability of the large-scale CO surveys. Therefore, the search for the gamma-ray sources could not take into account the granularity in the diffuse gamma-ray background due to the molecular hydrogen distribution (see Hermsen, 1980). Using the new detailed models of the diffuse gamma-ray distribution Pollock *et al.* (1985a, b) searched part of the galactic gamma-ray distribution for sources not explained by the gas and the empirical model for the cosmic-ray distribution. Work is in progress (Pollock *et al.*, 1988) to analyse the entire galactic plane region using the data and model presented in Section 2. The reality of the gamma-ray emission from the Vela and Crab pulsars was proven before the launch of COS-B, thanks to their timing signature (Crab, Parlier *et al.*, 1973; Vela, Thompson *et al.*, 1975). COS-B had these sources within its field of view for more than 200 days each, and results were presented earlier for the Crab pulsar by Bennett *et al.* (1977), Lichti *et al.* (1980), and Wills *et al.* (1982), and for the Vela pulsar by Bennett *et al.* (1977) and Kanbach *et al.* (1980). Detailed results on the spectral and temporal characteristics of the Vela gamma-ray emission (Grenier *et al.*, 1988) will be presented in Section 3 and these will be discussed in comparison with those of the Crab pulsar (Clear *et al.*, 1987).

## 2. The Radial Distribution of the Galactic Gamma Rays

The final COS-B database (Mayer-Hasselwander, 1985) contains a total of 65 observations, of which 55 include regions near to the galactic plane. The relative sensitivity of the instrument for these observations as well as the variations in the background with time during the COS-B mission was determined by Strong *et al.* (1987). Maps of the gamma-ray sky in three energy ranges, 70–150, 150–300, and 300–5000 MeV, are constructed using these data. These gamma-ray maps are correlated with HI maps,

derived from five different 21-cm line surveys (for references see Strong *et al.*, 1988), and maps of the integrated CO temperature, a composite of several surveys with the Columbia 1.2 m telescopes in New York City and on Cerro Tololo in Chile. The latter combined survey covers the entire galactic plane and is essentially complete up to ($|b| \sim 7$, with several large extensions to higher latitudes. The construction of H I column density maps and velocity-integrated CO maps for separate galacto-centric rings is described by Bloemen *et al.* (1986).

### 2.1. METHOD

The method consists of fitting the gamma-ray data to the function:

$$I_\gamma = \sum_i \frac{q_i}{4\pi} (\tilde{N}_{\mathrm{H\,I},\,i} + 2Y\tilde{W}_{\mathrm{CO},\,i}) + f_{\mathrm{IC}}\tilde{I}_{\mathrm{IC}} + I_B^0 + \sum_k f_k I_k \,, \tag{1}$$

where $q_i$ is the gamma-ray emissivity in the $i$th ring, $N_{\mathrm{H\,I},\,i}$ is the column density of atomic hydrogen, $W_{\mathrm{CO},\,i}$ is the velocity-integrated CO brightness temperature, $Y$ is the apparent gamma-ray value for the conversion factor from CO integrated temperature to $H_2$ column density (assuming that $q_i$ applies equally to atomic and molecular gas), $f_{\mathrm{IC}}I_{\mathrm{IC}}$ is the inverse Compton emission, $I_B^0$ is an isotropic background (cosmic + instrumental) corrected for temporal and angular variations (see Strong *et al.*, 1987, for details), $f_k$ is the flux of the $k$th point source included in the model, $I_k$ is the distribution for a source of unit strength situated at the $k$th source. The tilde indicates the convolution with the COS-B point-spread function, which is quite accurately known from pre-launch calibrations and studies of the Vela pulsar (see Hermsen, 1980 and Mayer-Hasselwander, 1985). The free parameters of the model are, for each energy range: $q_{i,\,i=1-6}$, $Y$, $f_{\mathrm{IC}}$, $I_B^0$, and $f_{k,\,k=1-4}$.

The galacto-centric rings chosen for the present analysis were: 2–4, 4–8, 8–10, 10–12, 12–15, and $>15$ kpc (taking $R_\odot = 10$ kpc). The choice of the 4–8 kpc ring is based on the wish to separate the main concentration of molecular gas in the inner galaxy.

The basic assumption characteristic of this method is that the gamma-ray emissivity is a function of radius only; no attempt is made explicitly to resolve non-axisymmetric structure in the emissivity distribution (e.g., related to spiral arms) or to distinguish arm/interarm emissivity contrasts. However, if contrasts are present, they will still be covered to some extent by the model via the $Y\tilde{W}_{\mathrm{CO},\,i}$ term, since the CO is at least in part a tracer of spiral structure. In this case the value of $Y$ derived from gamma rays will of course include the cosmic-ray contrast and, therefore, be an overestimate of the true $N_{\mathrm{H_2}}/W_{\mathrm{CO}}$ ratio factor, which we denote by '$X$'.

Equation (1) is valid for each range separately, but in this work Strong *et al.* (1988) study also cases where all energy ranges are considered together, in order to investigate models with energy-independent parameters. For example, the case of energy-independent shape for $q(R)$ and energy-independent $Y$ is treated by making fits to the three ranges simultaneously.

The inverse Compton emission was calculated using the model described in Strong *et al.* (1985a). However, the absolute level is determined via the free parameters $f_{IC}$ derived from fits to the gamma-ray data, and was found to be consistent with unity for all selected energy ranges.

The four most intense gamma-ray sources were explicitly included in the model via the final term. The sources are: the Vela pulsar, the Crab pulsar, Geminga (2CG195 + 04) and 2CG078 + 01. Note that the fluxes of these sources are free parameters, and the resulting spectra are interesting by-products of this analysis (given in Strong *et al.*, 1988).

The error analysis is performed using the information matrix technique described by Strong (1985b). The theoretical basis of the likelihood ratio method used is described in Bloemen *et al.* (1986), and a detailed treatment can be found in Kendall and Stuart (1973).

The fits were done principally for $|b| < 9.5°$, since the CO coverage is almost complete in this range. Since, however, the convolution means that coverage beyond this range is strictly necessary, most of the fits were also done with $|b| < 5.5°$ to check for differences. In this range the coverage is complete for the convolution but the statistics and dynamical range are smaller. Additional runs with $10° < l < 270°$ and $90° < l < 350°$ were done to check for differences between the 1st and 4th quadrants.

### 2.2. Fitting results

All parameters, error estimates and log-likelihood values for 11 different fits for the selected energy ranges 70–150, 150–300, and 300–5000 MeV are given in Strong *et al.* (1988). With these fits (i) the dependences of the parameters and likelihood values on the fitted region was tested; (ii) the requirement of an energy-dependent model was tested (energy dependence of $Y$ and/or the shape of the galacto-centric emissivity gradients); (iii) the requirement of a radial variation of $Y$ was tested. In this paper the main results will be discussed.

#### 2.2.1. *Fit Region*

The derived parameters were consistent within the quoted uncertainties, independent whether the wider or narrower latitude range was selected, and independent whether the first or fourth quadrant was excluded. Therefore, the results will be given for the total region ($|b| < 9.5°$, $10° < l < 350°$).

#### 2.2.2. *Energy Dependence*

The statistical tests indicated that the data require an energy-dependent model. Testing (i) an energy-dependent shape of $q(R)$ and an energy-independent $Y$ and (ii) an energy-independent $q(R)$ and energy-dependent $Y$, resulted in practically the same value for the likelihood indicating that the fit is 'equally good' in these two cases. However, the number of free parameters in the first case is larger, therefore the tests favour the second model: an energy-dependent $Y$ value. Thus, this model qualifies for the classification 'best' model. However, the energy dependence in this model is actually

due to a difference in $Y$ between the range 70–150 MeV and $>150$ MeV: $Y(70\text{–}150\ \text{MeV}) = (3.3 \pm 0.5) \times 10^{20}$ molecules cm$^{-2}$ (K km s$^{-1}$)$^{-1}$ and $Y(>150\ \text{MeV}) = (2.5 \pm 0.3) \times 10^{20}$ molecules cm$^{-2}$ (K km s$^{-1}$)$^{-1}$. This will be discussed in Section 2.2.4.

Figure 1(a–b) shows the radial dependence of the emissivity for the two models. The differences are within the quoted errors for each case. The main difference is in the inner galaxy at low energies (see the discussion in Section 2.2.4). The radial variation is smal as found by Bloemen *et al.* (1986), amounting to at most a factor 2 between the inner and outer galaxy, and 1.5 between the inner galaxy and the solar circle.

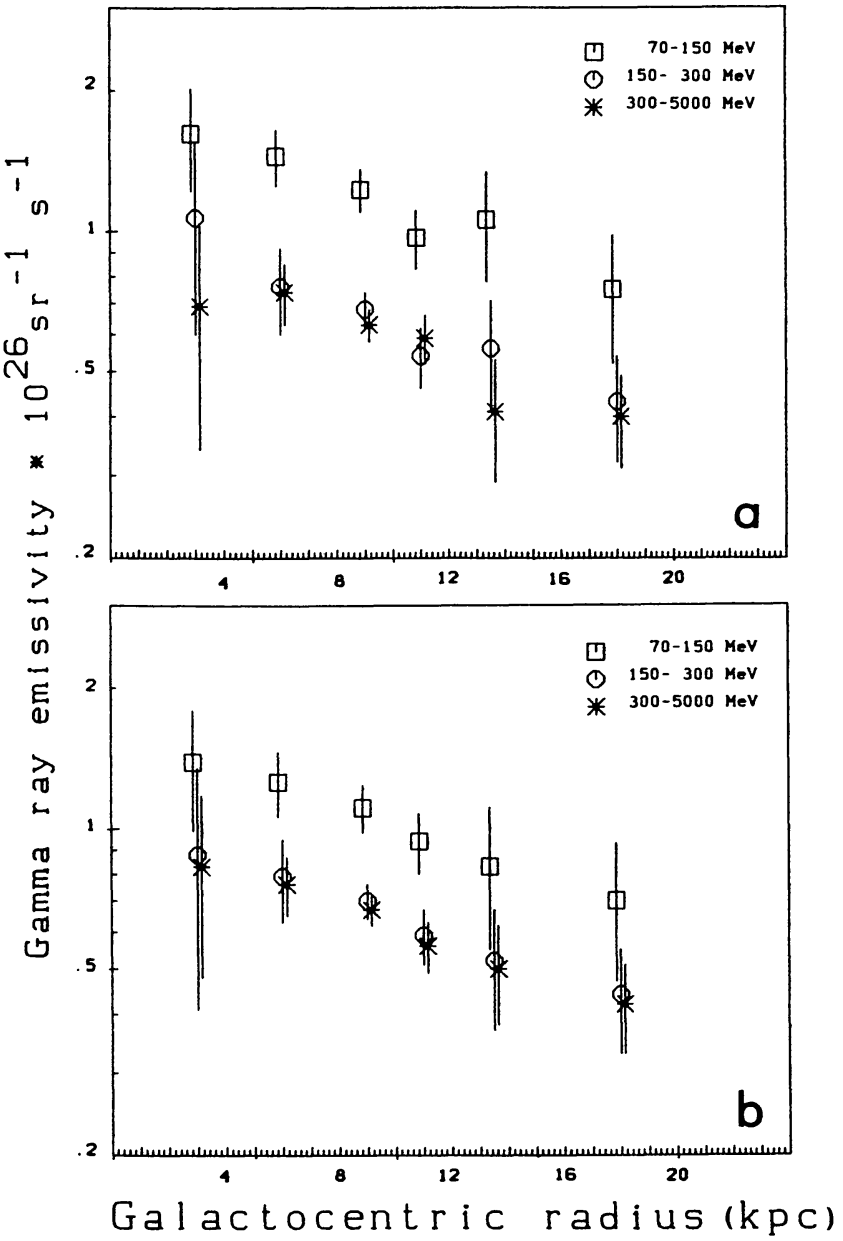


Fig. 1. Radial distribution of gamma-ray emissivity: (a) for $q(R)$ shape free, $Y$ energy-independent, case (i); (b) for $q(R)$ shape energy-independent, $Y$ energy-dependent, case (ii).

### 2.2.3. *The Value of the CO-to-$H_2$ Conversion Factor*

The choice of a 'best' value for the 'physical' conversion factor from CO integrated temperature to $H_2$ column density must depend on how one chooses to treat the fact that the fitted value of $Y$ in Equation (1) is larger at low energies (cf. case (ii)). Since $X$ is by definition energy-dependent, there are (at least) four possible situations:

(a) Systematic effects due to the poor angular resolution for 70–150 MeV.

(b) Other components (e.g., sources) with steep spectra which also correlate with the CO distribution.

(c) Effects related to cosmic-ray propagation or production in molecular clouds.

(d) Energy-dependent spiral arm/interarm cosmic-ray contrasts.

In each case it is clear that the value of $Y$ in the low-energy range is the least reliable indicator of $X$. The value also depends slightly on whether one assumes an energy-independent shape for $q(R)$ or not. The best estimate is made using cases (i) and (ii) for the 150–300 and 300–5000 MeV ranges; the value of $Y$ ranges from 2.0 to $2.5 \times 10^{20}$ molecules $\mathrm{cm}^{-2}$ $(\mathrm{K\ km\ s}^{-1})^{-1}$, so Strong *et al.* adopt $X = (2.3 \pm 0.3) \times 10^{20}$ molecules $\mathrm{cm}^{-2}$ $(\mathrm{K\ km\ s}^{-1})^{-1}$.

However, it should be kept in mind that this value is an upper limit if a population of unresolved gamma-ray point sources exists with an angular distribution similar to that of the molecular gas, or if the cosmic-ray density is enhanced in molecular clouds. A detailed discussion on the application of $X$ and a comparison with other determinations is given by Bloemen *et al.* (1986).

### 2.2.4. *Radial Variation of Y*

The effect of possible variations of $Y$ with $R$ was also tested against the gamma-ray data, particularly, since claims of substantial variation have been made together with the suggestion that this has a large effect on $q(R)$ (Bhat *et al.*, 1985a, b). For the two energy ranges above 150 MeV no significant difference was found in the value of $Y$ for $2 < R < 8$ kpc and $R > 8$ kpc, however, a factor 2 variation in $Y$ is improbable but not excluded. It is verified that such a variation would increase the gradient in $q(R)$ only slightly, leading to the conclusion that variations of $X$ in our Galaxy, even if present, do not have a major influence on our derived emissivity gradients.

The 70–150 MeV case is somewhat different showing a clear indication for $Y(2\text{–}8\ \mathrm{kpc})/Y(>8\ \mathrm{kpc}) > 1$ (formal significance $2 \times 10^{-3}$). In fact, essentially all the emission in the inner ring is attributed to the CO-like component, corresponding to a decrease in $q(R)$ in the inner galaxy; although not impossible *a priori*, it does seem very unlikely that such a sharp change in behaviour with respect to the higher energy ranges occurs. The uncertainty in $q(2\text{–}4\ \mathrm{kpc})$ and $q(4-5\ \mathrm{kpc})$ is clearly very large in this low-energy range; the reason for this is the difficulty in distinguishing the structures of the HI and CO in the data after convolution with the wide 70–150 MeV COS-B point-spread-function, which is somewhat uncertain in this energy range. Specifically, the inner galactic disk (inside $R = 8$ kpc) is not resolved below 150 MeV, so that the thickness of the predicted disk is sensitive to the adopted PSF width. A CO disk about

1° thick convolved with a 3.5° wide PSF has the same apparent thickness as a 2° wide H I disk convolved with a 3.0° wide PSF. While the sum of the H I and CO contributions is strongly constrained by the data, their ratio is highly uncertain in the inner galaxy at low energy. As long as the structures are resolved (as in the case outside 8 kpc for 70–150 MeV and everywhere at higher energies) the problem is minimized.

If we insist that $q(R)$ does not increase with $R$ at low energies, then consistency with higher energies is obtained: no radial variation of $Y$. However, some confidence is lost in our 'best' model (case (ii)), finding such a systematic effect at low energies.

### 2.3. Comparison of model with the observations

Figure 2 shows longitude distributions for $|b| < 5.5°$ for the 'best' model, corresponding to an energy-independent shape of $q(R)$ (case (ii)). The four fitted point sources are included in the plot. In this presentation the other case (i) appears almost indistinguishable from this one. Considering that systematic uncertainties in exposure can lead to fluctuations of up to 10% on top of the statistical noise, the fits are generally quite satisfactory, and show that the model is adequate to account for the bulk of the diffuse emission along the entire galactic plane.

Towards the inner galaxy, $|l| < 60°$, H I and $H_2$ produce approximately equal contributions to the gamma-ray intensity, indicating approximate equality of the mass in these components; our new estimate for the total mass of the molecular hydrogen in the inner galaxy (2–10 kpc) being $1.0 \times 10^9 M_\odot$.

Despite the general good agreement there are some significant deviations deserving attention. Most prominent is the galactic centre region, $|l| < 10°$, which is well known to deviate strongly from the behaviour along the rest of the galactic plane (Blitz *et al.*, 1985; Bania, 1986; Stacy *et al.*, 1987), and which was not included in the present fits for this reason. Stacy *et al.* (1987) have recently shown that this discrepancy may be accounted for by wide-line molecular clouds in the vicinity of the galactic centre.

Also prominent are the excesses in $330° < l < 345°$ for $> 300$ MeV. These are approximately coincident with the positions of the sources 2CG333 + 01 and 2CG342 – 02 (Swanenburg *et al.*, 1981). Also noticeable is the excess around 2CG135 + 01 and in the Carina region ($280° < l < 290°$). A significant dip visible at all energies around $60° < l < 70°$ corresponds to a well-known interarm region and may be the only hint in favour of an arm-interarm emissivity contrast.

### 2.4. Comparison with Bloemen et al. (1986)

In Bloemen *et al.* the first three galactic quadrants and the Carina region were used, and the analysis principle was the same as for these new results. It was concluded that $Y$ is energy-independent to within the accuracy of the analysis, while the shape of $q(R)$ was found to depend on energy. This was then interpreted as a steeper gradient for cosmic-ray electrons compared to nuclei. The new results confirm the small gradient at high energies, but ascribes the energy-dependence instead to the $Y$-value, although there may be some uncertainty in the analysis at low energies.

There are, therefore, some differences in the conclusions of these papers which require

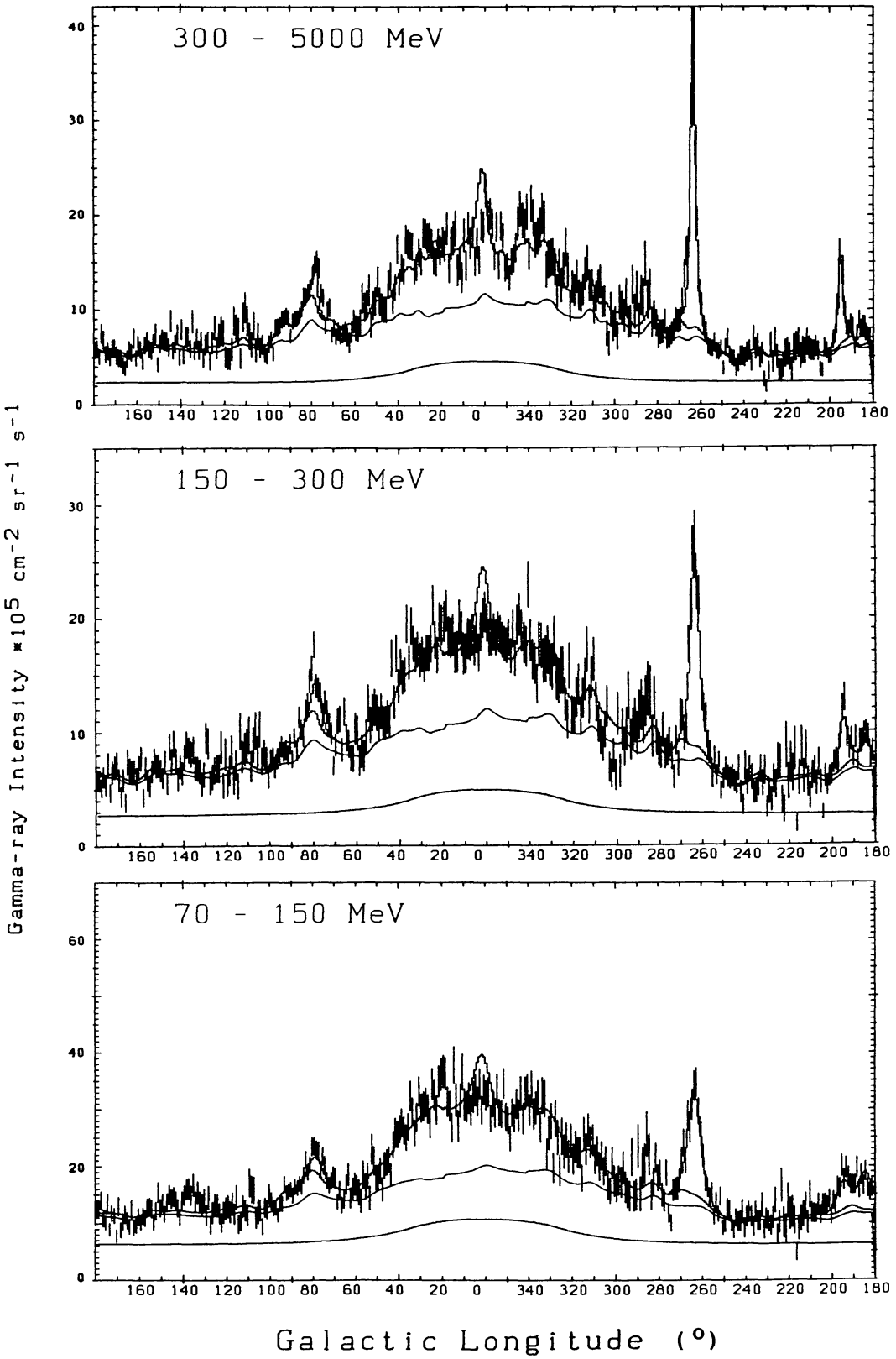


Fig. 2. Longitude distributions of predicted, model (ii), and observed gamma-ray intensities, averaged over $|b| < 5.5°$. *Vertical bars*: observed intensities $\pm 1\sigma$ error bars. *Continuous lines*: predicted intensities. *Lower line*: inverse Compton emission. *Middle line*: emission from H I. *Upper line*: total model, including H I, $H_2$, inverse Compton and four point sources. All predictions include the fitted isotropic background.

comment. In the first paper the energy-dependent $Y$ was stated as also acceptable. There is, therefore, no real inconsistency between the two analyses; the better data and treatment has produced a more reliable result. The improvements include the extension of the CO surveys to include the entire southern Galaxy, as well as extensive upgrading and filling-in for many other regions. Also, the final COS-B database with its additional observations and final corrections has been used.

### 2.5. Conclusions on the diffuse gamma-ray emission study

The diffuse galactic gamma-ray emission in the range 70–5000 MeV is well represented by the sum of contributions from atomic and molecular hydrogen with a small inverse-Compton component. The required emissivity gradient is small, with a maximum variation for the solar circle to inner galaxy of a factor 2. The gradient is much smaller than that of the distribution of supernova remnants or pulsars. Therefore, the arguments sometimes made invoking the gamma-ray gradient as direct support for cosmic-ray origin in such objects cannot be substantiated; cosmic-ray propagation effects have to be taken into account.

The 'best model' obtained is one in which $Y$ is energy-dependent, while the shape of the emissivity variation is energy-independent. The steeper gamma-ray spectrum towards the inner galaxy is then accounted by a $Y$-value increasing at low energies by about 40%. However, an energy-dependent emissivity variation fits the data, equally well, but our statistical tests indicate that it is less satisfactory when the number of degrees of freedom are taken into account.

A possible energy dependence of $Y$ is an interesting result perhaps related to physical processes associated with cosmic-ray propagation in molecular clouds, such as production of secondary electrons. Alternatively, steep-spectrum gamma-ray sources spatially correlated with clouds would give a similar effect.

Finally, it cannot be excluded that the energy-dependence of $Y$ is an artefact because our model is incomplete. In particular, cosmic-ray spectral variations as a function of distance from the galactic plane are not included in the model and would have a complicating effect. Indications for such variations, obtained from spectral-index studies of the COS-B data and radio-continuum data at 408 and 1420 MHz, have been presented by Bloemen (1987), Reich and Reich (1988), and Bloemen *et al.* (1988).

## 3. Temporal and Spectral Characteristics of the Vela Gamma-Ray Pulsar

The only radio pulsars detected in gamma rays so far are the young pulsars Crab and Vela. Recently, Clear *et al.* (1987) presented detailed results on the Crab pulsar using the final COS-B database; now also detailed results are available for the Vela pulsar (Grenier *et al.*, 1988). Prior to these new results, the experimental status can be summarized as follows: Tümer *et al.* (1984) at 0.3–30 MeV, Thompson *et al.* (1977) above 35 MeV, and Bennett *et al.* (1977) at 50 MeV–5 GeV all report a similar Vela lightcurve structure which is characterized by two sharp peaks separated by 0.42 in phase and bracketing the optical pulses. The energy spectrum of the pulsar still remains

uncertain. An extrapolation to X-ray energies of the COS-B results of Kanbach *et al.* (1980) lies several orders of magnitude above the reported upper limits, while at TeV energies the flux values reported by Bhat *et al.* (1980) clearly require a break in the spectrum. Earlier results from COS-B data by Bennett *et al.* (1977) and Kanbach *et al.* (1980) indicate a possible break in the spectrum at a few hundred MeV, but the level of significance of these results is low. This section presents the latest results on the Vela pulsar in the 50 MeV to 5 GeV energy range (Grenier *et al.*, 1988). The data have been collected using the COS-B satellite which observed the Vela region during 10 observation periods between October 1975 and June 1981. The total COS-B gamma–ray lightcurve together with the radio and optical ones are given in Figure 3.

### 3.1. The maximum likelihood method

A maximum likelihood analysis has been applied to the data to estimate the flux and spectral properties of the source. The newly developed approach (Grenier *et al.*, 1988)

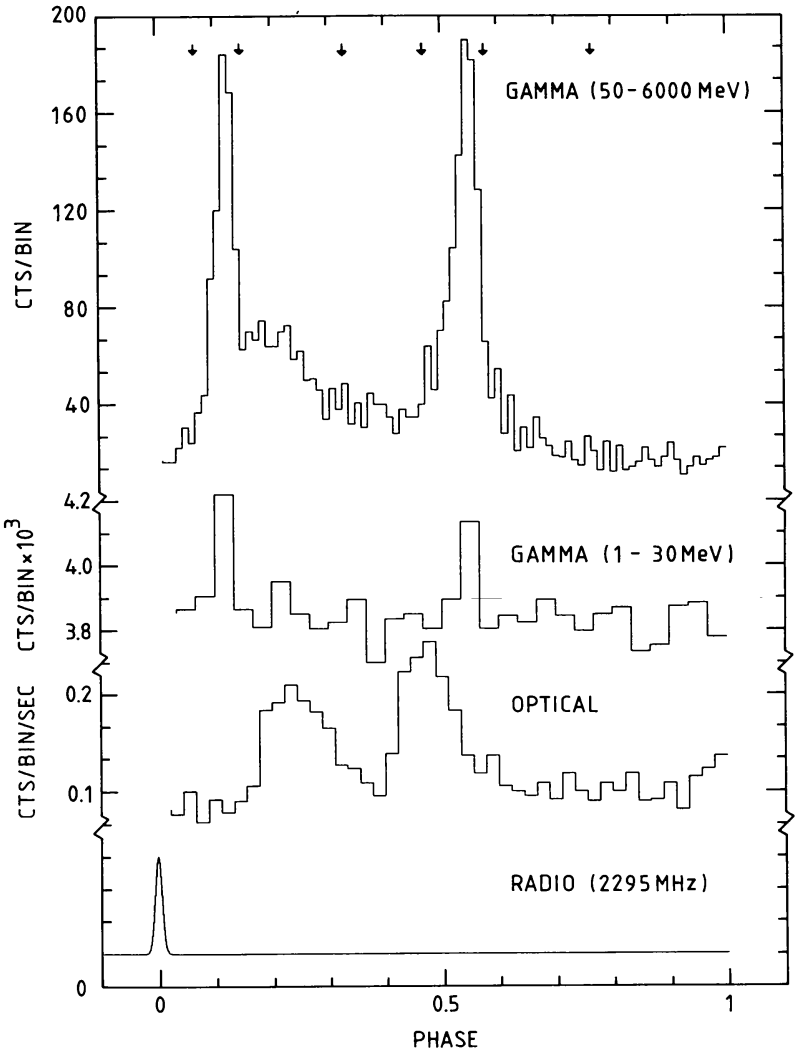


Fig. 3. The lightcurve from PSR 0833 – 45 at radio (Buccheri *et al.*, 1978), optical (Manchester *et al.*, 1980), soft energy gamma-rays (Tümer *et al.*, 1984), and high-energy gamma-rays (final COS-B). The arrows indicate the position of the phase boundaries which are used in this analysis.

utilizes all COS-B information, that is the arrival time, energy, and direction of each photon. It takes simultaneously into account the limited spatial and energy resolutions of the instrument, and their dependency on the inclination and energy of an event. Finally, it separates the pulsar emission from any background radiation by exploiting the pulsar lightcurve shape against the flatness of the background, and the source spatial structure (the COS-B point-spread-function) against the structure of the underlying diffuse emission originating in the interstellar medium and the isotropy of the instrumental noise. The statistical processing uses the maximum likelihood principle with a probability density function of detecting a photon at an energy $E_m$, position $l_m$, $b_m$, and phase $\phi_m$ (where $m$ is for 'measured' against 'true') expressed as:

$$\frac{\int_E \int_{lb} n(\phi, E. l, b)\, \mathrm{d}E\, \mathrm{d}\Omega\, \mathrm{CAL}(E_m, E, \alpha_{mlb}, \theta_{lb})}{\int_{E_m} \int_{l_m b_m} \text{Numerator}\, \mathrm{d}E_m\, \mathrm{d}\Omega_m} . \tag{2}$$

The true celestial gamma-ray distribution is described by $n(\phi, E, l, b)$. CAL represents the COS-B convolution, given by the product of its effective sensitive area, point-spread-function and energy resolution. These parameters have been determined from pre-launch calibration data (Hermsen, 1980; Mayer-Hasselwander, 1985). $\theta_{lb}$ represents the true inclination angle with respect to the detector axis of the photons coming from a point source at $(l, b)$ and reconstructed at an angle $\alpha_{ml,\,b}$ away from this source. $\Omega$ denotes the solid angle. The likelihood value can then be computed from the product of the probabilities of finding the photons actually recorded by COS-B.

For the Vela gamma-ray source, the general model to test may include up to four major components:

(1) The pulsed emission from the pulsar: $F_{vp}(\phi)E^{-\gamma_p(\phi)}\,\delta(l - l_v, b - b_v)$.

(2) A possible steady component from Vela: $F_{vs}E^{-\gamma_s}\,\delta(l - l_v, b - b_v)$.

(3) A constant and isotropic instrumental background: $B_I E^{-\gamma_i}$.

(4) The steady diffuse galactic emission around the pulsar: $qN_{\mathrm{H}}(l, b)E^{-\gamma_g}$.

The latter term results from the interaction of cosmic rays with interstellar matter ($N_{\mathrm{H}}$ is the total hydrogen column density). Its spatial structure can be traced by H I and CO surveys, as has been shown in Section 2.

Testing different models is performed by evaluating the likelihood expression for the parameters of the different components: $B_I$, $q$, $F_{vs}$, $F_{vp}(\phi)$, and the different spectral slopes: $\gamma_i$, $\gamma_g$, $\gamma_s$, $\gamma_p(\phi)$. The highest likelihood value gives the most probable model for $n(\phi, E, l, b)$ that explains the data.

Table I gives the details of the phase domains which have been selected for the analysis. The background region (phase 0.77–0.07) has been analysed for possible steady emission from Vela. The resultant upper limit shows that such emission accounts for less than a few percent of the pulsed luminosity, and may thus be neglected from

TABLE I

Definition of the selected intervals of the Vela lightcurve

| Region | Phase interval |
|---|---|
| Peak 1 | 0.07–0.15 |
| Interpulse-1 | 0.15–0.33 |
| Interpulse-2 | 0.33–0.47 |
| Peak 2 | 0.47–0.58 |
| Trailer | 0.58–0.77 |
| Background | 0.77–0.07 |

the model. Ignoring possible steady emission in the model implies that outside the pulsed phase range, the photons only come from the two background components of the model. As a first step the likelihood analysis is performed for the events from the background phase domain to give the best emissivities and spectral indices of the instrumental background and galactic emission ($B_I$, $\gamma_i$, $q$, $\gamma_g$). These values are then fixed in the model and the analysis is applied to the photons from the other five phase intervals independently to derive the emissivities $F_{vp}(\phi)$ and spectral indices $\gamma_p(\phi)$ of the pulsed emission within each selected phase. For those observations with large source aspect angles ($> 15°$), where the efficiency and the energy resolution of the instrument are poor, this likelihood analysis is limited by the available statistics and has not been performed. For the remaining observations a detailed analysis has been made for the 5 phase intervals. Within each phase interval the analysis has been performed for 3 energy intervals (50–5000, 50–300, and 300–5000 MeV). The division of the data into these energy intervals is based on the indication for a break in the pulsed spectrum at approximately 300 MeV found in the analysis of Kanbach *et al.* (1980) using only 2 observations. Due to computing time considerations the position of the spectral break has not been used as an additional free parameter within the model, however, the results of the independent modelling of the spectrum above and below 300 MeV strongly support this choice of value.

### 3.2. Results

The likelihood analysis has been performed for the 5 selected phase intervals, for the 5 best observation periods and for 3 energy ranges, giving a total of 75 spectra and flux values. Only the main results will be highlighted (for detailed results see Grenier *et al.*).

#### 3.2.1. *Total Pulsed Flux*

The spectrum of the whole emission derived independently at energies above and below 300 MeV and using all observations is:

$$F(50 \leq E \leq 300 \text{ MeV}) = (2.74 \pm 0.21) \times 10^{-4} E_{\text{MeV}}^{-1.72 \pm 0.07} \text{ ph cm}^{-2} \text{ s}^{-1} \text{ MeV}^{-1},$$

$$F(300 \leq E \leq 5000 \text{ MeV}) = (2.71 \pm 0.04) \times 10^{-3} E_{\text{MeV}}^{-2.12 \pm 0.07} \text{ ph cm}^{-2} \text{ s}^{-1} \text{ MeV}^{-1}.$$

The significant difference between the high- and low-energy spectral indices clearly shows that the time-averaged Vela pulsed spectrum from 50 to 5000 MeV cannot be described by a single power law. At least two are required and in this representation the good connection between the two spectra at 300 MeV strongly supports the choice of 300 MeV as the energy of the break. The flux of the pulsed emission from Vela has been determined by integrating the two-power-law phase averaged spectrum for each observation. The result, displayed in Figure 4(a), indicates the striking long-term variability of Vela. In addition, the likelihood analysis provides simultaneously the background intensity for each observation, and its stable behaviour from one observation to the next, displayed in Figure 4(b), confirms the true source origin of the pulsed variability phenomenon. To study the energy dependence of this variability, Figure 5 shows the evolution of the pulsed flux for the energy ranges 50–300 and 300–5000 MeV.

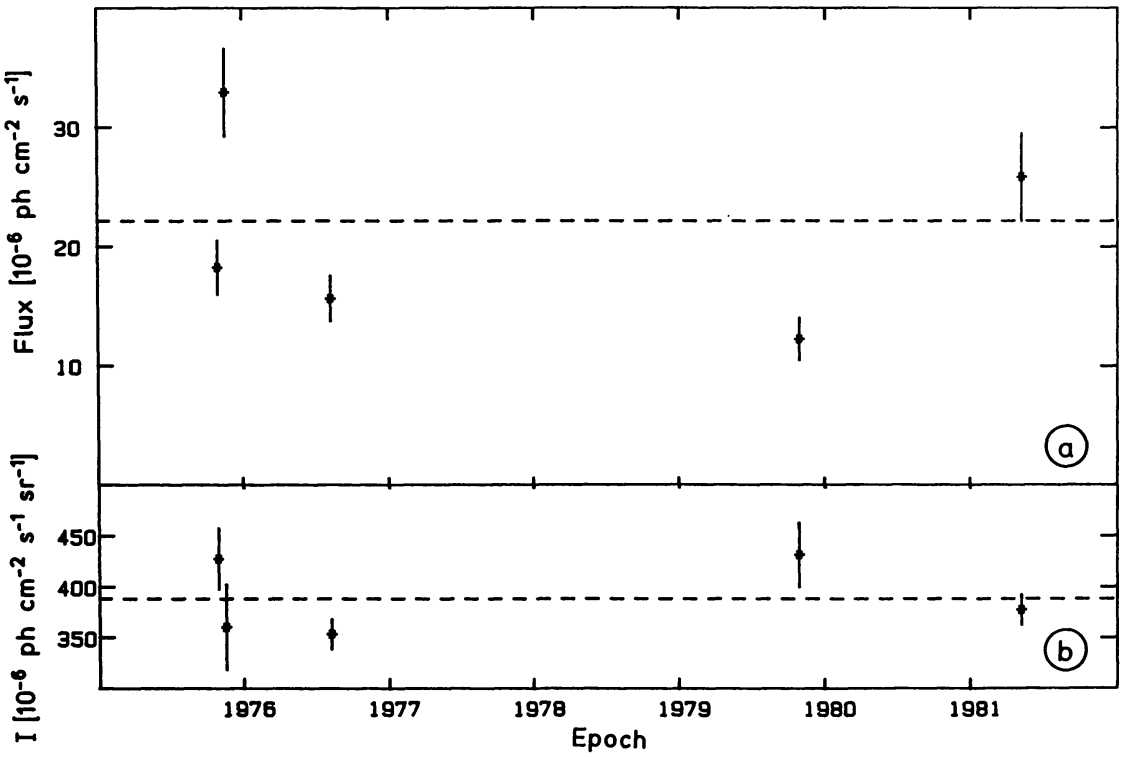


Fig. 4. Integrated gamma-ray flux/intensity ($I$) values (50–5000 MeV) calculated using the likelihood analysis for 5 observations from 1975 to 1982. (a) The pulsed gamma-ray flux for PSR 0833 – 45; (b) the diffuse galactic background and instrumental emission.

The main contribution to the flux variability is clearly due to the low-energy emission. The different evolutions of the flux from the two energy ranges denote a distortion of the Vela spectrum from one epoch to the next. The observed fluctuation in the spectral ratios (the ratio of low- to high-energy flux) has a probability of $10^{-10}$ of being due to a random effect.

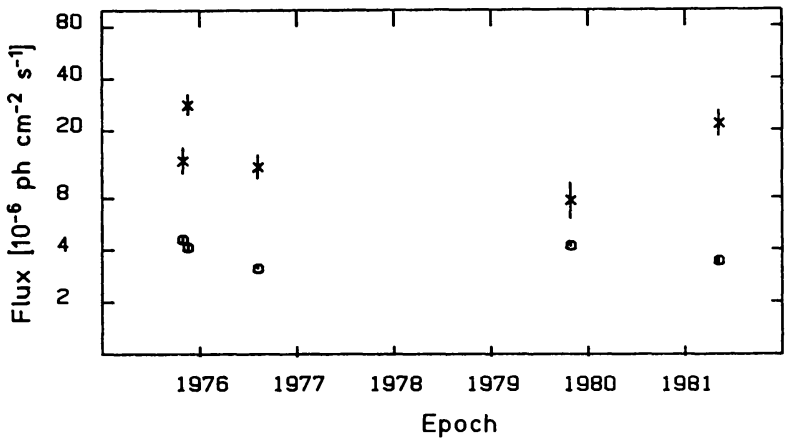


Fig. 5. Vela pulsed gamma-ray flux values integrated over 50–300 MeV ( × ) and 300–5000 MeV (○) for the same observation periods as in Figure 4.

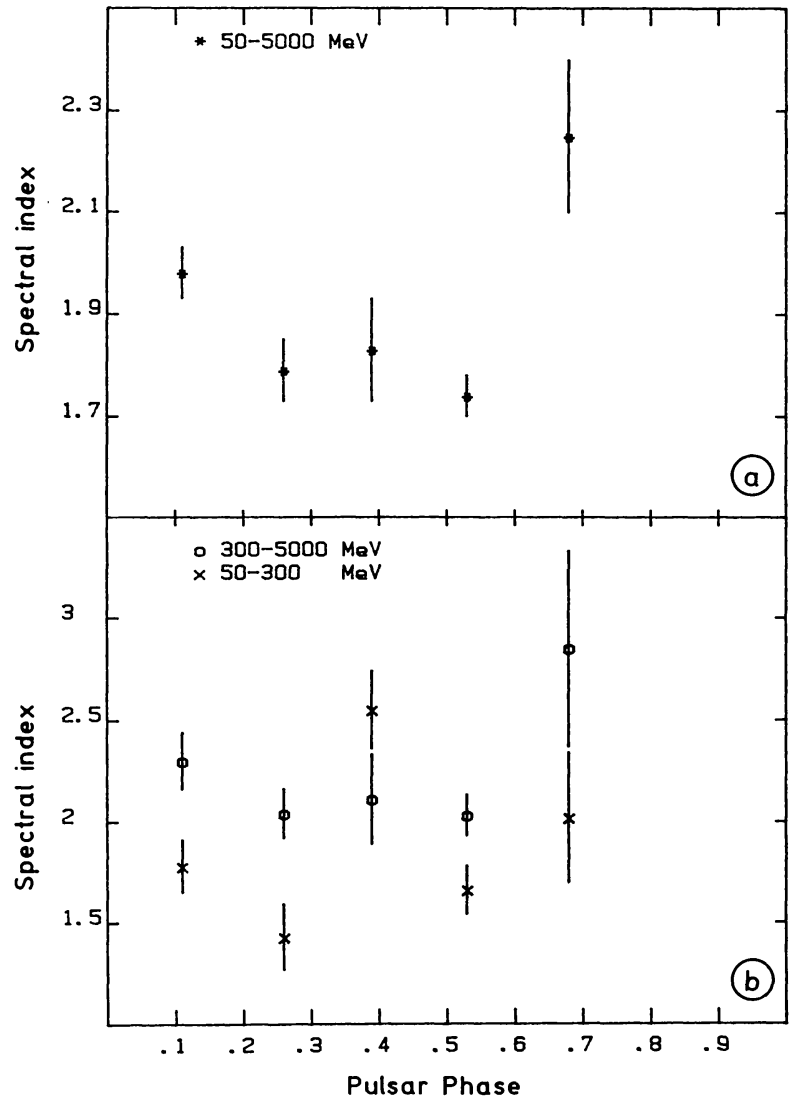


Fig. 6. Time-averaged pulsed spectral index as a function of phase; (a) one-power-law fit over total energy range; (b) for high- and low-energy ranges.

### 3.2.2. *Spectra for Different Phase Intervals*

Figure 6(a) shows the time-averaged spectral index as a function of phase. The probability that the emission may be best represented by a homogeneous spectrum over all phases ($E^{-1.84}$) is $10^{-4}$. A further understanding of the phase dependency of the pulsed emission may be obtained from Figure 6(b), which shows the spectral characteristics of the high- and low-energy emissions as a function of phase. Analysis of the spectral characteristics of the high-energy emission shows that there is no significant variation in its spectral index with phase, giving a phase-averaged value of $2.12 \pm 0.07$. Thus, the spectral index of the GeV radiation from Vela displays both a stable and homogeneous behaviour. In contrast, the spectral index of the low-energy emission shows evidence for phase dependence (chance probability $5 \times 10^{-3}$). It is evident from the change in the spectral index at low energies (from the first peak to interpulse-2, $4.5\sigma$, and interpulse-2 to the second peak, $3.6\sigma$ and from the softness of the first peak and trailer over the entire energy range, that 5 separate phase components exist in the Vela gamma-ray lightcurve.

### 3.2.3. *Flux Variability for Separate Phase Components*

The evolution of the flux from each of the phase components for each observation and for both high- and low-energy ranges has been studied. The long-term variability is obvious and the relative amplitude of the variability is significantly larger for the two interpulse emissions. Furthermore, the flux variations in the separate energy intervals are different resulting in spectral distortions (probability levels are given in Grenier *et al.*, 1988). To illustrate their long-term evolution, the energy spectra giving the maximum likelihood fits to the data for each observation are displayed in Figure 7. Good agreement is observed between the low- and high-energy fits at approximately 300 MeV for most phase components. The two-power-law representation is, therefore, a good approximation to the real spectra (for the trailer, the poor statistics make interpretation of the results rather difficult). The actual position of the break or bend in the real spectrum will vary somewhat in energy following the apparent long-term variability.

### 3.2.4. *Total PSR 0833 – 45 Spectrum*

The two-power-law fit time-averaged spectrum of the whole pulsed emission has been plotted in Figure 8 together with the data recorded at other wavelengths in order to show the full energy distribution of the Vela pulsed radiation over the entire electromagnetic spectrum. Over this spectrum, the pulsar reaches its maximum luminosity in the MeV–GeV domain. At very high energies the recent results of Bhat *et al.* (1987) indicate a spectral slope of $-3.5$ at TeV energies which does not require an excessive steepening when extrapolating over three decades of energy from the COS-B gamma-ray range. The observed time variability presented in this article may support the proposed time variability at TeV energies, e.g., Bhat *et al.* (1980), however, it should be noted that the variations recorded above a few hundred MeV are relatively small ($\lesssim 25\%$). The very low upper limits set by the Einstein and HEAO 1 satellites (energy ranges 0.1–4.5 and

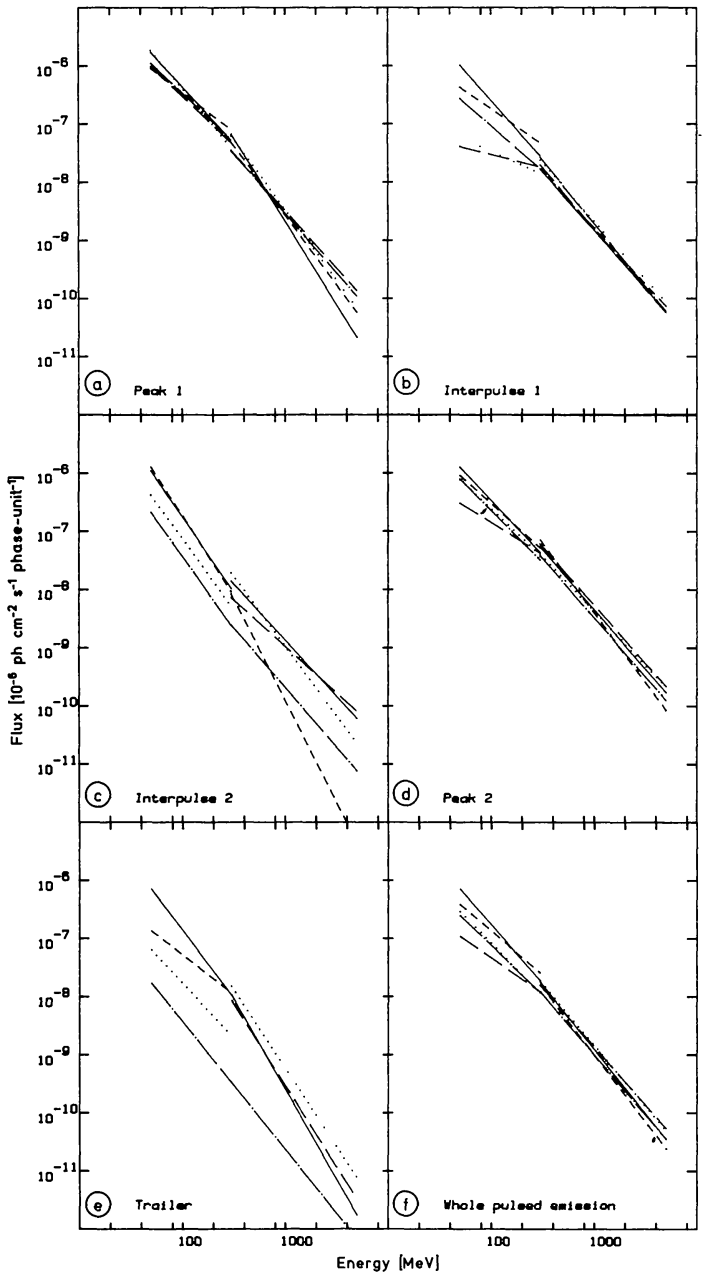


Fig. 7. Differential pulsed gamma-ray spectra (50–5000 MeV) from Vela for 5 phase intervals and the total phase-averaged emission. The power-law spectra giving the maximum likelihood fits are shown for the 50–300 MeV and 300–5000 MeV energy ranges, respectively, for each observation; period 2 ....., period 3 ——, period 12 –.–.–, period 45 – –, period 59 ---.

15–175 keV) suggest that the energy distribution in the X-ray domain is still bending before rising again towards the optical and radio wavelengths.

### 3.2.5. *Long-Term Time Variability of PSR 0833 – 45*

The flux evaluation presented in Figure 4(a) demonstrates the gamma-ray variability of the pulsar over several years. Figure 9(b) shows the same data points together with flux values measured by COS-B when Vela was seen at large inclination angles, and the Vela

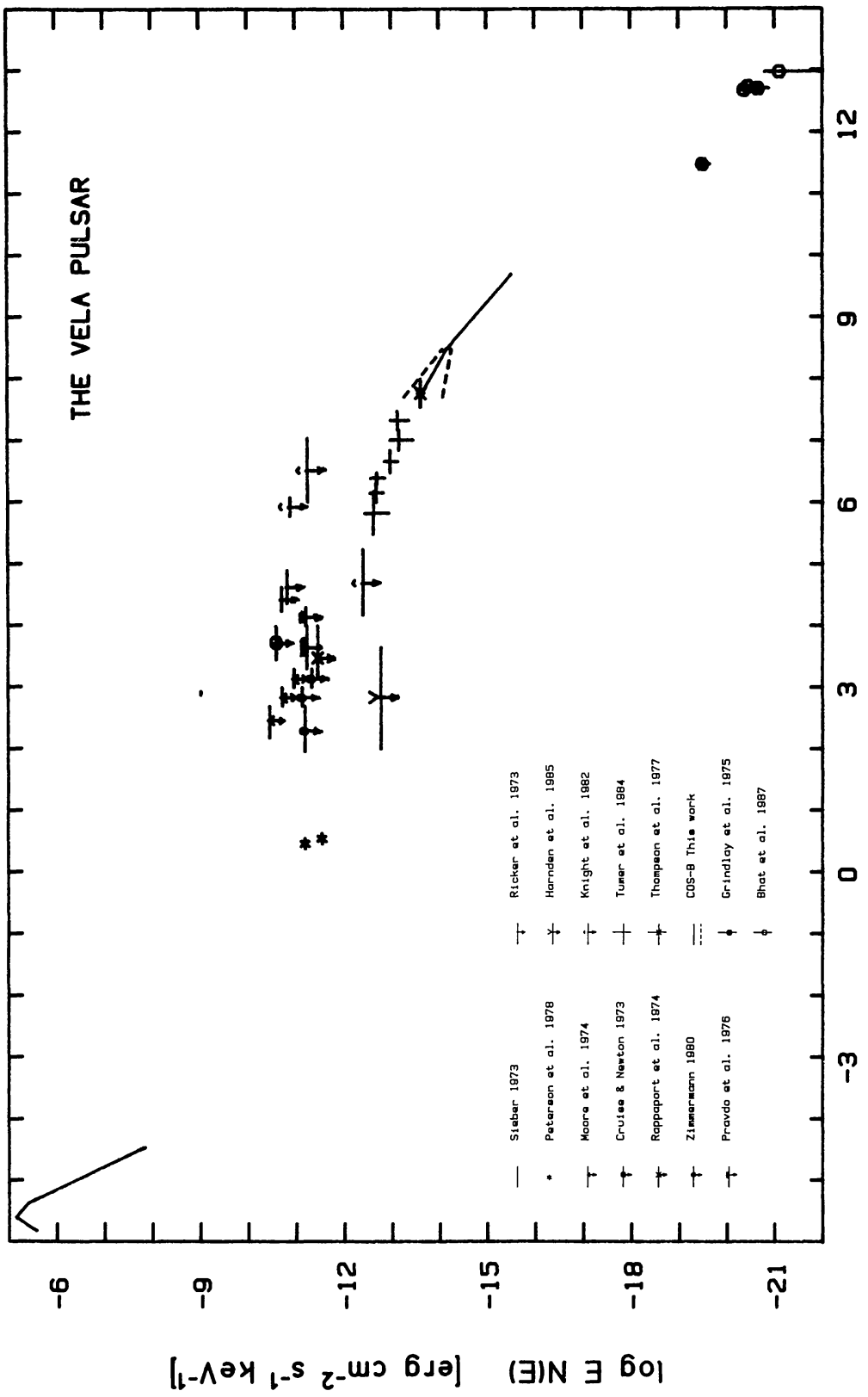


Fig. 8. Total energy spectrum from the radio up to the very high-energy gamma-ray domain. The upper limits ($3\sigma$) displayed in the X-ray range are calculated for an assumed duty cycle of 0.2 similar to the optical one. The broken lines indicate the extremities in the variabilities measured by COS-B between 50 and 300 MeV.

flux measured by SAS-2 in 1973. A large discontinuity in the pulsar rotational parameters, a so-called glitch, occurred sometime between September 25 and October 15, indicated in Figure 7 (Manchester *et al.*, 1976), while the COS-B gamma-ray observations started on October 20. This could indicate a relation between the gamma-ray flux with an exponential risetime of $\sim 11$ days and decay time of $\sim 140$ days, and the glitch event. However, the recurrence of such a phenomenon may be questioned. A further glitch occurred in July 1978 (Downs *et al.*, 1978) when no COS-B data were taken from the source (see Figure 9). According to the time-scales quoted above, a coincident gamma-ray flux increase could have happened without being noticed in later COS-B observations. What is surprising, is the high gamma-ray flux recorded in April and May 1981 when no glitch was reported. Such an event occurred five months later, in October 1981 (Gorenstein *et al.*, 1981), when Vela was not in the field-of-view. Thus, the gamma-ray enhancement is recurrent but it does not necessarily follow a glitch event. For this reason, it is not possible to draw any firm conclusion from the COS-B data on the relationship between the gamma-ray variability and the glitch phenomenon.

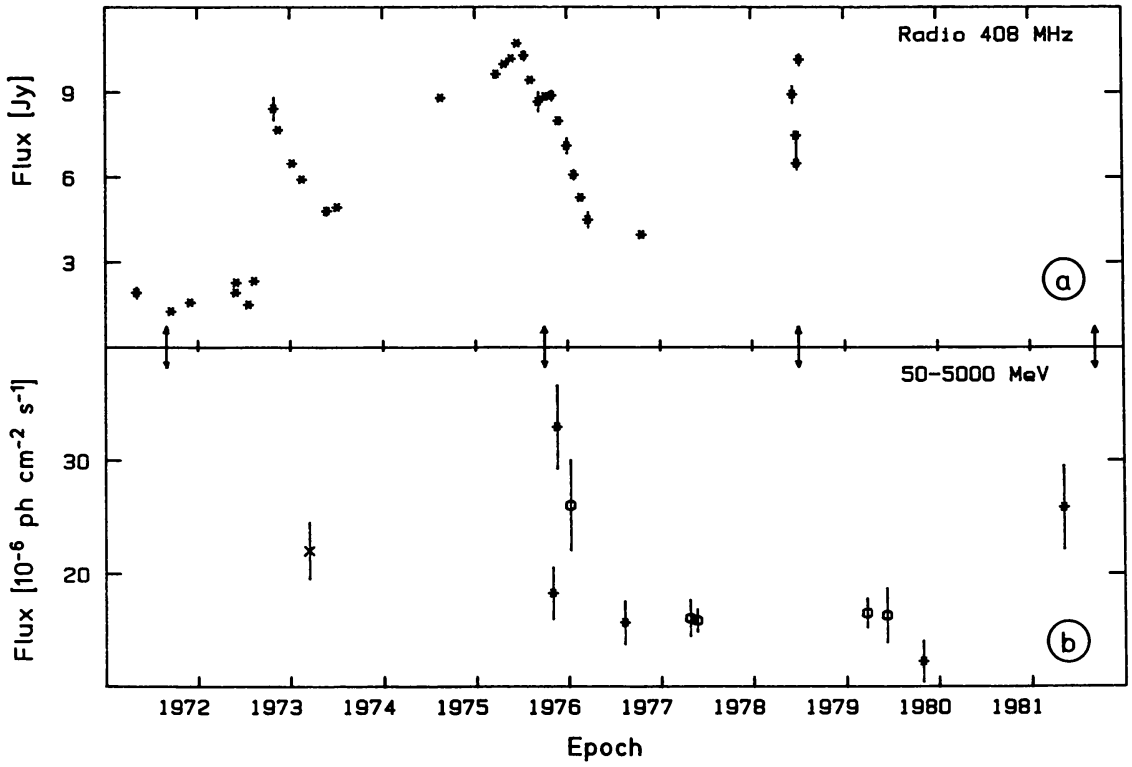


Fig. 9. Comparison between the evolution of the radio flux (a) at 408 MHz (McAdam, 1981) and the high-energy gamma-ray flux (b) for the Vela pulsar. Gamma-ray data points: *, COS-B likelihood analysis; ○, COS-B saturation method; ×, SAS-2 (Thompson *et al.*, 1977). The epochs of the pulsar glitches are indicated.

The Vela pulsed radio flux is not stable either. As shown in Figure 9(a), three large irregularities were recorded at 408 MHz between 1971 and August 1978 when the observations at the Molonglo Observatory were stopped (McAdam, 1981). These

secular changes could not be explained by the interstellar scintillation, nor do they appear to be related to the glitches. Their rather regular aspect over the years suggested that such fluctuations are caused by a precession in the beam angle with respect to our line-of-sight (McAdam, 1981). Despite the minimal overlap of the radio and the gamma-ray data, one could conclude that the two variation patterns are not strongly correlated. Therefore, the precession effect proposed for the radio evolution is not supported by the gamma-ray data, since in this case it would not explain the stability of the first peak while the other phase components all vary. No other clues to the origin of the long-term variability can be found from the pulsed emission at other wavelengths. In the optical band, the 24th magnitude Vela object is too faint to provide so far precise information on possible apparent magnitude changes.

## 4. Crab versus Vela Characteristics and Some Model Implications

### 4.1. Crab versus Vela

The detailed gamma-ray results on the Vela pulsar, presented in the previous section, can be compared with the COS-B results from a detailed analysis of the high-energy gamma-ray emission from the Crab pulsar (Clear *et al.*, 1987). First, it is reminded, that the Crab pulsar is the only pulsar seen to emit pulsed radiation over a range of $\sim 20$ decades in frequency, while the Vela pulsar is only detected in the radio, optical, and gamma-ray domain. Furthermore, it was found that the Crab pulsar reaches its maximum luminosity in the hard X-ray range till soft gamma-ray, while the Vela pulsar reaches its maximum luminosity in the few-hundred-MeV range. The relatively low X-ray emissivity of the Vela pulsar is in clear contrast to that of the Crab pulsar. In the high-energy gamma-ray domain (50 MeV to about 5 GeV) the spectrum of the Crab pulsar emission can be represented by a single power law of index $2.00 \pm 0.10$ and no systematic variations of spectral index with pulsar phase have been noted (three components in the Crab lightcurve were compared: first peak, interregion, and second peak). The differences with the spectrum of the Vela pulsar emission are evident: the Vela spectrum cannot be represented by a single power law and the spectrum varies significantly with pulsar phase.

The striking similarity between the appearances of the two gamma-ray lightcurves, both dominated by two peaks separated in phase by about 0.42, holds only for the gamma-ray range. The Vela lightcurves have been shown in Figure 3; in the case of the Crab the two peaks in the lightcurves in the optical, X-ray and gamma-ray (up to a few GeV) domains are coincident to within the timing errors, and coincide with the main radio pulse and interpulse. In the latter domain below 1 GHz there is also a separate component, known as the 'precursor' (Rankin *et al.*, 1970); this is similar in shape, spectrum, and polarization to the radio pulse of Vela.

Finally in Section 2 strong flux and spectral long-term variability of the Vela gamma-ray emission was evidenced; in the case of the Crab only marginal long-term variability has been noted in the flux ratio of the two pulses (Clear *et al.*, 1987). Particularly

remarkable is the strong variability in the Vela interpulse emission. Furthermore, the Vela pulsar showed long-term variability in its radio emission. Other radio pulsars have proved to be variable sources as well, but usually on a much shorter time-scale. In the Crab case, after a continuous weakening of the 74 MHz pulsed emission was observed between 1971 and 1975, its radio flux remained steady over the next six years (Rickett and Seiradakis, 1982), as did its optical and X-ray flux (Knight, 1982). Hence, in the long-term, the Vela and Crab pulsars do behave differently and the large variability observed from Vela, both in radio and gamma-rays, looks unusual to the measured behaviour of all other pulsars.

### 4.2. Implications for some pulsar models

Many models have been proposed to explain how pulsed radiation can be produced at different wavelengths within a pulsar magnetosphere. Many agree on the existence of accelerating regions called 'gaps', which arise from a local charge depletion and provide the primary population of ultra-relativistic particles streaming along the magnetic field lines. However, the models disagree on the location of the active regions (e.g., polar gaps, outer gaps, etc.). In Grenier *et al.* (1988) the implications of the new Vela results on some models for the Vela pulsar are discussed; here the discussion is limited to a geometrical model which has been evaluated by Morini (1983) for the Vela pulsar and further by Smith (1986) for the Crab and Vela pulsar together.

Morini and Smith evaluated a schema in which the magnetic dipole is assumed to be orthogonal to the rotation axis and the two main gamma-ray pulses are produced in the two sets of the terminal field lines above the same pole and close to the light cylinder. The Vela radio pulse and the Crab precursor are produced at the opposite pole. This scheme assumes that the photons are emitted along the field lines, and shows that the arrival phases of the photons depend on the radii, between the star surface and the light cylinder, at which they are created. They show that the differences in the spectra between the two Vela gamma-ray peaks may come from the phase reconstruction. Only those photons created near the leading terminal field lines close to the light cylinder contribute to the first peak. On the other hand, 'outer' photons from the trailing side may combine with photons from the same field lines deeper in the magnetosphere and also with photons from the polar cap region to produce the second peak with its harder gamma-ray spectrum. Furthermore, the geometrical pattern indicates that for Vela the optical pulses are produced in the open magnetosphere above the pole, at a distance which is about half the light cylinder radius, and that the gamma-ray interpulses originate along the same lines at a slightly higher altitude. The mixing in interpulse-2 of photons created well inside the magnetosphere and near the polar cap could again explain the spectral differences with interpulse-1. The synchronisation of the pulses in the Crab lightcurve from the optical to the gamma-ray range indicates that they are all emitted close to the light cylinder along the outer gap (Smith, 1986). Also, the similarity of the spectra of the two peaks, indicates that for the Crab the geometry of the magnetic field lines is somewhat different, excluding a significant contribution in the second peak from regions deeper into the magnetosphere.

The long-term variability of the Vela gamma-ray lightcurve also implies different source locations for the highly variable interpulse emissions and for the relatively stable main peaks. In the model presented by Smith, the various evolutions observed for the different gamma-ray components in the Vela lightcurve would signify that the region sensitive to the variability is the open magnetosphere in the polar region, while the conditions along the last open field lines in the outer magnetosphere would be more steady. This agrees with the steadiness of the Crab pulsar emission at all wavelengths.

For Vela, the details of the radio pulse profile and polarisation involve a source located close to the star cap (Krishnamohan and Downs, 1983). Therefore, the variability observed in radio supports the idea that the conditions in the inner magnetosphere may change in the long-term. The same conclusion is reached when considering that the largest contribution to the variability in the gamma-ray domain comes from the low-energy part, provided that in the cascade of photons the softer originate from deeper into the magnetosphere.

The qualitative discussions of the new aspects of the gamma-ray emission in these geometrical models proposed by Morini and Smith suggests that the origin of the interpulses exists above one of the poles, deep in the magnetosphere or at medium latitudes, with the sources of the peaks lying close to the co-rotating magnetosphere and to the light cylinder.

## 5. Concluding Remarks

Five years after the end of the COS-B orbital operations still new and interesting results are being derived from the large COS-B database. The new results on the large-scale properties of the diffuse gamma radiation, cosmic-ray distribution, and galactic matter distribution provide a solid basis for future investigations by GAMMA-1 and the GRO mission. The availability of detailed surveys of tracers of the molecular hydrogen distribution over large areas of the sky enabled the COS-B correlation studies, mainly after the gamma-ray measurements. The future missions, studying the diffuse emission, can benefit from the start, also in their search for point sources. Particularly for weak sources, close to their detection thresholds, a detailed modelling of the granular underlying emission is important. Even in a study of a strong source such as the Vela pulsar, the inclusion of the galactic background model in the analysis might increase the reliability in obtaining detailed characteristics, as has been shown in Section 3. The latter interesting results on gamma-ray pulsars give an indication of the exiting results which we can expect from the future missions.

## Acknowledgements

The results presented in this paper reflect the success of a collaborative effort lasting many years. Particularly, I would to thank my colleagues of the former COS-B Caravane Collaboration Hans Bloemen, John Clear, Isabelle Grenier, François Lebrun, Andy Pollock, and Andrew Strong who showed the courage and endurance to continue the analysis which led to these detailed findings.

## References


Bania, T. M.: 1986, *Astrophys. J.* **308**, 868.

Bennett, K., Bignami, G. F., Boella, G., Buccheri, R., Hermsen, W., Kanbach, G., Lichti, G. G., Masnou, J. L., Mayer-Hasselwander, H. A., Paul, J. A., Scarsi, L., Swanenburg, B. N., Taylor, B. G., and Wills, R. D.: 1977, *Astron. Astrophys.* **61**, 279.

Bhat, P. N., Gupta, S. K., Ramana Murthy, P. V., Sreekantan, B. V., Tonwar, S. C., and Viswanath, P. R.: 1980, *Astron. Astrophys.* **81**, L3.

Bhat, P. N., Gupta, S. K., Ramana Murthy, P. V., Sreekantan, B. V., Tonwar, S. C., and Viswanath, P. R.: 1987, *Astron. Astrophys.* **178**, 242.

Blitz, L., Bloemen, J. B. G. M., Hermsen, W., and Bania, T. M.: 1985, *Astron. Astrophys.* **143**, 267.

Blitz, L., Fich, M., and Stark, A. A.: 1980, in B. Andrew (ed.), *Interstellar Molecules,* D. Reidel Publ. Co., Dordrecht, Holland, p. 213.

Bloemen, J. B. G. M.: 1987, *Astrophys. J.* **317**, L15.

Bloemen, J. B. G. M., Reich, P., Reich, W., and Schlickeiser, R.: 1988, *Astron. Astrophys.*, in press.

Bloemen, J. B. G. M., Strong, A. W., Blitz, L., Cohen, R. S., Dame, T. M., Grabelsky, D. A., Hermsen, W., Lebrun, F., Mayer-Hasselwander, H. A., and Thaddeus, P.: 1986, *Astron. Astrophys.* **154**, 25.

Buccheri, R., Caraveo, P. A., D'Amico, N., Hermsen, W., Kanbach, G., Lichti, G. G., Masnou, J. L., Wills, R. D., Manchester, R. N., and Newton, L. N.: 1978, *Astron. Astrophys.* **69**, 141.

Clear, J., Bennett, K., Buccheri, R., Grenier, I. A., Hermsen, W., Mayer-Hasselwander, H. A., and Sacco, B.: 1987, *Astron. Astrophys.* **174**, 85.

Cruise, A. M. and Newton, A. C.: 1973, *Nature Phys. Sci.* **244**, 121.

Dame, T. M., Ungerechts, H., Cohen, R. S., de Geus, E., Grenier, I., May, J., Murphy, D. C., Nyman, L.-A., and Thaddeus, P.: 1987, *Astrophys. J.* **322**, 706.

Dogiel, V. A. and Uryson, A. V.: 1988, *Astron. Astrophys.* **197**, 335.

Downs, G. S., Manchester, R. N., and Newton, L. M.: 1978, *IAU Circ.,* 3274.

Gordon, M. A. and Burton, W. B.: 1976, *Astrophys. J.* **208**, 346.

Gorenstein, M. V., Shapiro, I. I., Rogers, A. E. E., and Cohen, N. L.: 1981, *IAU Circ.,* 3644.

Grenier, I. A., Hermsen, W., and Clear, J.: 1988, *Astron. Astrophys.*, in press.

Grindlay, J. E., Helmken, H. F., Hanbury-Brown, R., Davis, J., and Allen, L. R.: 1975, *Astrophys. J.* **201**, 82.

Harnden, F. R., Jr. and Gorenstein, P.: 1973, *Nature* **214**, 107.

Hermsen, W.: 1980, Ph.D. Thesis, Univ. Leiden.

Kanbach, G., Bennett, K., Bignami, G. F., Buccheri, R., Caraveo, P., D'Amico, N., Hermsen, W., Lichti, G. G., Masnou, J. L., Mayer-Hasselwander, H. A., Paul, J. A., Sacco, B., Swanenburg, B. N., and Wills, R. D.: 1980, *Astron. Astrophys.* **90**, 163.

Kendall, M. G. and Stuart, A.: 1973, *The Advanced Theory of Statistics*, Vol. II, Charles Griffin and Co., London.

Knight, F. K.: 1982, *Astrophys. J.* **260**, 538.

Knight, F. K., Matteson, J. L., Peterson, L. E., and Rotschild, R. E.: 1982, *Astrophys. J.* **260**, 553.

Krishnamohan, S. and Downs, G. S.: 1983, *Astrophys. J.* **265**, 372.

Kulkarni, S. R., Blitz, L., and Heiles, C.: 1982, *Astrophys. J.* **259**, L63.

Lichti, G. G., Buccheri, R., Caraveo, P., Gerardi, G., Hermsen, W., Kanbach, G., Masnou, J. L., Mayer-Hasselwander, H. A., Paul, J. A., Swanenburg, B. N., and Wills, R. D.: 1980, in R. Cowsik and R. D. Wills (eds.), *Non-Solar Gamma Rays, Advances in Space Exploration*, Vol. 7, Pergamon, Oxford, p. 49.

Manchester, R. N., Goss, W. M., and Hamilton, P. A.: 1976, *Nature* **259**, 291.

Manchester, R. N., Wallace, P. T., Peterson, B. A., and Elliot, K. H.: 1980, *Monthly Notices Roy. Astron. Soc.* **190**, 9P.

Mayer-Hasselwander, H. A.: 1985, *Explanatory Supplement to the COS-B Database,* ESTEC, Noordwijk, The Netherlands.

McAdam, W. B.: 1981, *Proc. Astron. Soc. Australia* **4**, 219.

Moore, W. E., Agrawal, P. C., and Garmire, G.: 1974, *Astrophys. J.* **189**, L117.

Morini, M.: 1983, *Monthly Notices Roy. Astron. Soc.* **202**, 495.

Parlier, B., Agrinier, B., Forichon, M., Leray, J. P., Boella, G., Maraschi, L., Buccheri, R., Robba, N. R., and Scarsi, L.: 1973, *Nature Phys. Sci.* **242**, 117.

Peterson, B. A., Murdin, P. G., Wallace, P. T., Manchester, R. N., Penny, A. J., Jorden, A., King, D., and Hartley, K. F.: 1978, *Nature* **276**, 475.,

Pollock, A. M. T., Bennett, K., Bignami, G. F., Bloemen, J. B. G. M., Buccheri, R., Caraveo, P. A., Hermsen, W., Kanbach, G., Lebrun, F., Mayer-Hasselwander, H. A., and Strong, A. W.: 1985a, *Astron. Astrophys.* **146**, 352.

Pollock, A. M. T., Bennett, K., Bignami, G. F., Bloemen, J. B. G. M., Buccheri, R., Caraveo, P. A., Hermsen, W., Kanbach, G., Lebrun, F., Mayer-Hasselwander, H. A., and Strong, A. W.: 1985b, *Proc. 19th Int. Cosmic Ray Conf., La Jolla* **1**, 338.

Pravdo, S. H., Becker, R. H., Boldt, E. A., Holt, S. S., Rothschild, R. E., Serlemitsos, P. J., and Swank, J. H.: 1976, *Astrophys. J.* **208**, L67.

Rankin, J. M., Comella, J. M., Craft, H. D., Richards, D. W., Campbell, D. B., and Counselman, C. C.: 1970, *Astrophys. J.* **162**, 707.

Rappaport, S., Bradt, H., Doxsey, R., Levine, A., and Spada, G.: 1974, *Nature* **251**, 471.

Reich, P. and Reich, W.: 1988, *Astron. Astrophys.*, in press.

Ricker, G. R., Gerassimenko, M., McClintock, J. E., Ryckman, S. G., and Lewin, W. H. G.: 1973, *Astrophys. J.* **186**, L111.

Rickett, B. J. and Seiradakis, J. H.: 1982, *Astrophys. J.* **256**, 612.

Smith, F. G.: 1986, *Monthly Notices Roy. Astron. Soc.* **219**, 729.

Stacy, J. G., Dame, T. M., and Thaddeus, P.: 1987, *Proc. 20th Int. Cosmic Ray Conf.* **1**, 117.

Strong, A. W.: 1985a, *Astron. Astrophys.* **145**, 81.

Strong, A. W.: 1985b, *Astron. Astrophys.* **150**, 273.

Strong, A. W., Bloemen, J. B. G. M., Hermsen, W., Lebrun, F., Mayer-Hasselwander, H. A., and Buccheri, R.: 1987, *Astron. Astrophys. Suppl.* **67**, 283.

Strong, A. W., Bloemen, J. B. G. M., Dame, T. M., Grenier, I. A., Hermsen, W., Lebrun, F., Nyman, L.-A., Pollock, A., and Thaddeus, P. A.: 1988, *Astron. Astrophys.*, in press.

Swanenburg, B. N., Bennett, K., Bignami, G. F., Buccheri, R., Caraveo, P. A., Hermsen, W., Kanbach, G., Lichti, G. G., Masnou, J. L., Mayer-Hasselwander, H. A., Paul, J. A., Sacco, B., Scarsi, L., and Wills, R. D.: 1981, *Astrophys. J.* **243**, L69.

Szabelski, J., Mayer, C. J., Richardson, K. M., Rogers, M. J., and Wolfendale, A. W.: 1987, *Proc. 20th Int. Cosmic Ray Conf.* **1**, 133.

Thompson, D. J., Fichtel, C. E., Kniffen, D. A., and Ögelman, H. B.: 1975, *Astrophys. J.* **200**, L79.

Thompson, D. J., Fichtel, C. E., Kniffen, D. A., and Ögelman, H. B.: 1977, *Astrophys. J.* **214**, L17.

Tümer, O. T., Dayton, B., Long, J., O'Neill, T., Zych, A., White, R. S.: 1984, *Nature* **310**, 214.

Wills, R. D., Bennett, K., Bignami, G. F., Buccheri, R., Caraveo, P. A., Hermsen, W., Kanbach, G., Masnou, J. L., Mayer-Hasselwander, H. A., Paul, J. A., and Sacco, B.: 1982, *Nature* **296**, 723.

Zimmerman, H. V.: 1980, *Astron. Astrophys.* **88**, 309.